This is the accepted manuscript made available via CHORUS. The article has been published as:

Time-resolved differential transmission in MOVPE-grown ferromagnetic InMnAs

M. Bhowmick, T. R. Merritt, G. A. Khodaparast, Bruce W. Wessels, Stephen A. McGill, D. Saha, X. Pan, G. D. Sanders, and C. J. Stanton

Phys. Rev. B **85**, 125313 — Published 27 March 2012

DOI: 10.1103/PhysRevB.85.125313

Time Resolved Differential Transmission in MOVPE Grown Ferromagnetic InMnAs

M. Bhowmick, T. R. Merritt, G. A. Khodaparast*
Department of Physics, Virginia Tech, Blacksburg, VA 24061, USA

Bruce W. Wessels
Materials Research Center, Northwestern University, Evanston, IL, 60208, USA

Stephen A. McGill
National High Magnetic Field Laboratory Florida, Tallahassee, FL.

D. Saha, X. Pan, G. D. Sanders, C. J. Stanton
Department of Physics, University of Florida, Gainesville, FL 32611
(Dated: February 3, 2012)

We measured time-resolved differential transmissions in InMnAs for different pump/probe schemes as a function temperature, laser fluence, and external magnetic fields. We observed tunability of the carrier relaxation time. In addition, we found that the sign of the differential transmission changed as a function of probe wavelength. The electronic structure for InMnAs was calculated for $\mathbf{B} = 0$, using an 8 band $\mathbf{k}\cdot\mathbf{p}$ model which includes conduction and valence band mixing as well as the coupling of the electrons and holes to the ferromagnetic Mn impurities. This allows us to determine the spin splitting of the bands at zero magnetic field and also explain some of the carrier dynamics and the sign changes in the differential transmission.

PACS numbers:

1. INTRODUCTION

Narrow gap ferromagnetic semiconductors (NGFS) such as InMnAs have significant potential for applications in infrared spin photonics and in spin transport devices due to their small energy gap, and much higher electron and hole mobility than other III-Mn-V ferromagnetic semiconductors. The first III-V NGFS, InMnAs, was prepared by MBE with a Curie temperature T_c on the order of 10 K. Subsequent fabrications demonstrated a T_c closer to 90 K[1]. A low temperature MBE technique was nearly exclusively used to prepare InMnAs thin films; although, MOVPE, an alternative technique demonstrated that single phase magnetic InMnAs compound could be deposited at 500° C, much higher than that used in MBE[2,3] .

Furthermore, the MOVPE technique demonstrated that the films are ferromagnetic with a T_c of 330 K[3,4]. The Rudermann-Kittel-Kasuya-Yosida (RKKY) mechanism, where free holes mediate the ferromagnetism, is indeed favored in NGFS while a small hole effective mass m_h results in a long interaction distance and effective exchange coupling. The hole effective Bohr radius in NGFS suggests a large enough overlap with the Mn induced hole wave functions to stabilize ferromagnetism even for small Mn contents[5]. The samples' ferromagnetic states were measured using several techniques reported earlier[2–4,6].

In this work, several time resolved differential transmission (TRDT)[7–9] schemes were employed to provide insight into the time scales and the nature of the interactions in MOVPE grown ferromagnetic InMnAs. We demonstrate the sensitivity and tunability of the carrier dynamics to the initial excitation region as well as the final states which are probed. The MOVPE grown InMnAs structure, is an 800 nm thick film with a Mn content of $\sim 4\%$, a hole concentration $p = 1.35 \times 10^{18} cm^{-3}$, and a mobility of 142 cm^2/Vs with the T_c above room temperature. The details of the growth conditions are described in Refs. 3,4. Probing the dynamical behavior of nonequilibrium carriers created by intense laser pulses can provide valuable information about different scattering mechanisms and the band structure. Time resolved spectroscopy can help us to understand the relaxation of photoexcited carriers; where after the initial excitation, the nonequilibrium population of electrons and holes can relax by a series of scattering processes including, carrier-carrier and carrier-phonon scattering.

Most of the understanding of carrier relaxation in MBE grown narrow gap (III,Mn)V ferromagnetic structures has been based two color differential reflectivity spectroscopy with pump and probe pulses ranging from 1.2-2 μm and 650-850 nm, respectively[10–13]. In the reported measurements, rapid change of the differential reflectivity was observed and ascribed to a fast disappearance of photoinduced free carriers through ultrafast trapping by mid-gap states. The carrier relaxation time reported in the MBE grown InMnAs[12] demonstrated a similar time scale as an InAs film under similar experimental conditions[14]. Fast relaxation in the differential reflectivity patterns of relaxation dynamic are commonly seen in low-temperature-grown III-V semiconductors.The ex-

---

*Author to whom correspondence should be addressed; Electronic address: `khoda@vt.edu`

tracted information from the differential reflectivity measurements can be affected by multi-reflections in multilayer structures.

It is important to emphasize and note that our studies are unique in being able to investigate carrier dynamics in ferromagnetic semiconductors. That is because our InMnAs samples are on a GaAs substrate. Photoexcitation by the 800 nm pump pulse creates the majority of carriers in the InMnAs part of the sample with only a few carriers being excited near the band edge in the GaAs layer. In contrast, previously InMnAs[12] was grown on a GaSb buffer layer. Photoexcitation by the pump probe created substantial carriers in this buffer layer making it difficult to separate out the relaxation dynamics of the magnetic InMnAs layer from the GaSb buffer layer. In addition, GaMnAs samples are grown on a GaAs substrate. Photoexcitation by the pump pulse creates carries both in the GaMnAs layer as well as the GaAs substrate and again, one can not separate out the relaxation dynamics of the carriers in the magnetic layer from that in the non-magnetic layer. We demonstrated the tunability of carrier dynamics and relaxation time with characteristics not reported in the MBE grown InMnAs[12] and InAs[14], the examples of our measurements are presented here.

2. DEGENERATE DIFFERENTIAL TRANSMISSION

In our degenerate TRDT pump/probe measurements, the laser source was a Difference Frequency Generator (DFG), which mixes the signal and idler beams from an Optical Parametric Amplifier (OPA). The OPA itself was pumped by an amplified Ti:sapphire oscillator with a repetition rate of 1 KHz. The pulses had a duration of ∼ 100 fs defining the resolution of the measurements with the ratio of the pump:probe of 1000:1. Both beams were focused onto the sample with a spot size of around 150-200 μm for probe and slightly larger for the pump. The differential transmissivity as a function of the time delay between the pump and probe pulses was measured using a liquid N2-cooled MCT detector.

Figure 1a shows examples of our degenerate TRDT in the InMnAs film with 4% Mn content. The photoexcited carriers were generated/probed at 3.467 μm, close to the fundamental gap of InMnAs, at 290 K and 77 K and several relaxation regimes, after the initial increase in the DT were observed. Optical transitions in semiconductors can be strongly influenced by the distribution of carriers in the conduction and valence bands. The initial sharp increase in the DT results from free carrier Drude absorption; whereas, the alteration of the dielectric function of the film through changes in the electron and hole distribution function can be responsible for the sign change of the Differential Transmission (DT). As shown in Fig. 1b, by tuning the pump/probe at 3.1 μm, the DT demonstrated a different pattern and at 77 K the photoexcited carriers, in the time scale of ∼ 2 ps, fully relaxed to its initial value at negative time delay.

In the presence of point defects and mid-gap states, nonlinear absorption dynamics can influence the relaxation process, where the observed fast decay could be due to trapping of carriers in the mid gap states and the slow component could be reflecting the slow recombination of the trapped carriers. In addition, in a degenerate pump-probe scheme when the pump/probe excitations are from the same source, the optical excitation of the carriers, followed by the fast relaxation in the bands, can result in a saturation of the band-to-band absorption[15,16]. In order to avoid possible nonlinear effects we employed a non-degenerate differential transmission and examples of the measurements are presented.

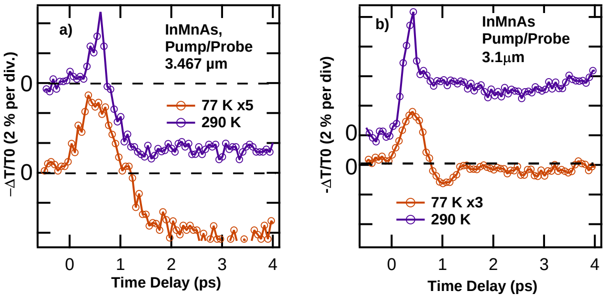

FIG. 1: a) DT in MOVPE grown ferromagnetic InMnAs at 290 K and 77 K with pump/probe fixed at 3.467μ m. b) A different pattern in the relaxation was observed for the pump/probe at 3.1 μm.

3. NON-DEGENERATE DIFFERENTIAL TRANSMISSION

In our Non-Degenerate Differential Transmission (NDDT) scheme the pump pulses were tuned above the fundamental gap. In this scheme, the photoexcited carriers were created by NIR pulses fixed at 800 nm above the InMnAs fundamental gap and probed by laser pulses ranging from 1.3-3.8 μm. The pump fluence was tunable from 1-5 mJ-cm^{-2} corresponding to a photoexcited carrier density in the range of $\sim 1\times10^{18}-5\times10^{19} cm^{-3}$; respectively. The band structure calculations, presented in section 4, show the optical transitions for a pump wavelength of 800 nm.

Figure 2 demonstrates the two-color differential transmission measurements in InMnAs ferromagnetic film at 290 K for different pump fluences. The fast component of the temporal evolution can be attributed to the relaxation of the hot electrons and holes, and the slower component is attributed to the electron-hole recombination across the gap. In the regime of high electron densities, due to the screening effect and hot phonons, the hot electrons experience a significant reduction in their energy loss rate through the emissions of LO phonons; therefore, the relaxation time of the hot electrons increase at

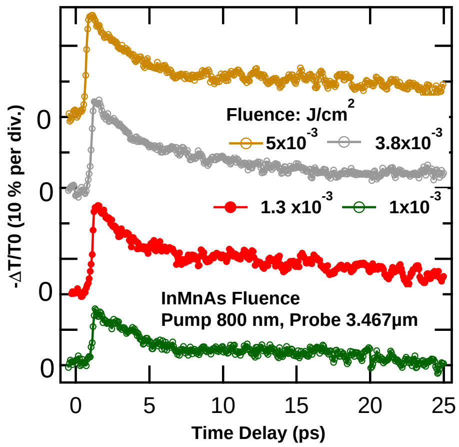

FIG. 2: Two-color differential transmission measurements in InMnAs ferromagnetic film at 290 K and different pump fluences. The pump/probe pulses were 800 nm and 3.467 μ m, respectively. the peak of the DT, $-\Delta T/T_0 = (T_0 - T)/T_0$, increases from 30% to $\sim$ 60%, suggesting larger photoinduced absorption at higher laser fluences.

higher laser fluences[17]. In addition, some of the photoexcited electrons energetically able to scatter between the X, L, and Γ valleys in the conduction band resulting in a longer and more complex relaxation dynamics[18,19]. The threshold for L-Valley scattering this sample is discussed in section 4.

The reabsorption of the trapped carriers in the mid gap levels are responsible for the long relaxation time of the observed photoinduced absorption[20,21]. The photoexcited electrons in the conduction band can return to the valence band through the defect and mid-gap states. The trapped electrons act as additional absorption center and could be reexcited to the conduction band after absorbing the probe beams. Except for the lowest laser fluence, the photoinduced carriers were not fully relaxed in a time scale longer than 10 ps.

As shown in Fig. 3, for the pump fixed at 800 nm, and a fluence of 3.8 mJ-cm^{-2}, tuning the probe wavelengths in MIR resulted in several differences in the TRDT patterns, where both the amplitude and the relaxation time demonstrate strong wavelength dependence. The $-\Delta T/T_0$ change, at 3.0 μm exceeded 60 %, suggesting larger photoinduced absorption compared to 3.8 μm in which the band filling could be more dominating. The gradual increase in the amplitude of TRDT peak as a function of the wavelength originated from the band-gap renormalization important for probe energies around the band gap.

Demonstrated in the inset of Fig. 3, lowering the temperature to 77 K increased the relaxation time. If the reexcitation of the trapped electrons can influence and increase the relaxation of the photoinduced carriers, then the thermal fluctuations at higher temperatures make it harder to trap the photogenerated electrons, resulting in a faster relaxation compared to the observation at 77 K.

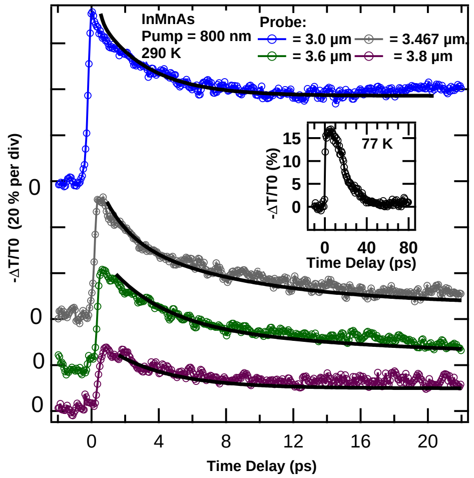

FIG. 3: Two-color differential transmission measurements in InMnAs ferromagnetic film at 290 K for different probe wavelengths in MIR. The relaxation dynamic is dominated by photoinduced absorption. The exponential fits are shifted for clarity. the inset demonstrates an example of the measurements at 77 K for pump/probe at 800 nm/3.467 μm, respectively.

Our observations in the NDDT scheme in InMnAS were dominated by photoinduced absorption only for the wavelengths longer than 2.6 μm. For several NIR probe pulses, ranging from 1.3 to 2.6 μm, we instead observed photoinduced bleaching. Figure 4 demonstrates examples of the photoinduced bleaching at different temperatures in InMnAs for the pump/probe tuned at 800nm/2μm, respectively. The temperature dependence of the observed photoinduced bleaching is not strong and the relaxation in this case lasts longer than the photoinduced absorption process. Due to the *Pauli exclusion* principle,photoexcited electrons in the conduction band and holes in the valence band can reduce the interband optical transitions via band and state filling. This leads to a decrease in the absorption, and a corresponding increase in the transmission, which is referred to as bleaching. In a study by Kim *et al.*[21], the sign of the differential reflectivity demonstrated a wavelength dependence in GaMnAs structures where point defect induced absorption is a possible mechanism .

While the TRDT is sensitive to the initial states and the band structure, we have tested a scheme where the photoexcited carriers were generated by pumping the GaAs substrate followed by a similar measurement on the ferromagnetic layer side. As shown in Fig. 5 the nature of the relaxations are different suggesting the strong dependence of the dynamics to the characteristics of the system under study. Unlike the case for Fig. 5a, in Fig. 5b the carriers are excited from the GaAs and experienced different relaxation process compared with carriers originating from the ferromagnetic layer.

The observed wavelength dependence motivated us to

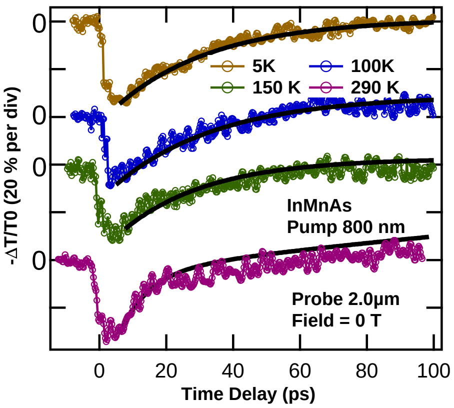

FIG. 4: Two-color DT measurements of InMnAs ferromagnetic film, at several temperatures. The pump/probe pulses were 800 nm and 2 μm. The photoinduced bleaching is dominating the temporal evolution of the DT.

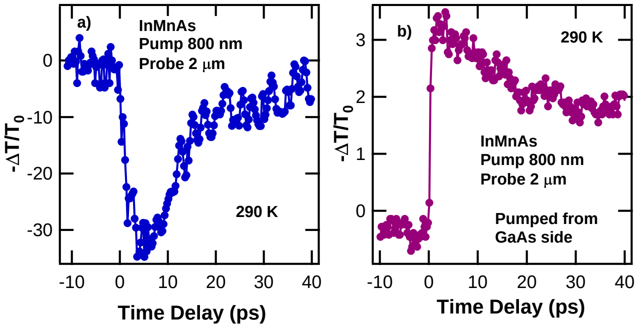

FIG. 5: Two-color DT measurements of the InMnAs ferromagnetic film in two different configurations and relaxation dynamics. a) When the film is pumped from the ferromagnetic side b) When the film is pumped from the GaAs side

probe the possibility of tuning the nature of the relaxation dynamics in the presence of external magnetic fields. In this case, the optical components inside the magnet were only compatible for probe pulses tuned below 2 μm with the pump pulses at 800 nm. Examples of our measurements at 5 K are presented in Fig. 6, where the photoinduced bleaching mainly dominated the temporal evolution of the DT. For external fields of 5 T and 10 T, the photoinduced bleaching changes sign at a time delay of $\sim$ 40 ps. Tuning the wavelengths around the band edge ($3.0 - 3.8 \mu m$) did not result in any change in the DT; however, applying an external field of 5 Tesla, where the band structure is more complicated, caused the switch in the sign.

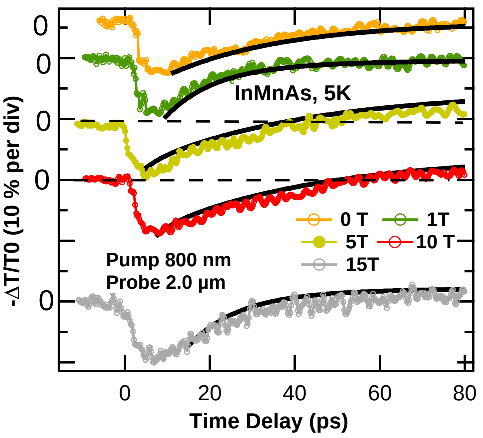

FIG. 6: Two-color DT signals from InMnAs at different applied fields at 5 K. The exponential fits are shifted for clarity.

4. CALCULATION OF ELECTRONIC STRUCTURE

To understand the effects of the ferromagnetic order on the electronic structure and subsequently the carrier relaxation dynamics, the electronic structure for bulk InMnAs has been calculated. Our preliminary calculations have focused on the band structure. By calculating the electronic band structure, we can determine where photoexcited carriers are generated by the pump pulse and which regions of the electronic structure are sampled by the probe pulse. Later we will focus on the carrier dynamics. The calculations are based on an 8 band k·p model which includes the conduction and valence band mixing. The model is similar to the Pidgeon-Brown model which we have previously used to calculate electron states and to interpret cyclotron resonance experiments. In this situation however, there is *no external magnetic* field but we allow for k_x and k_y dependence. We use the standard eight $\mathbf{k}$ =0 Bloch basis states (two spin states each for the conduction band, heavy-hole, light hole and spin-split valence band states) with no external magnetic field. We however include the effects of the spontaneous magnetization of the Mn ions and the *sp-d* coupling of this magnetization to the electrons and holes. This will spin-split the bands even with no external magnetic field, provided the Mn ions are ferromagnetically ordered. The magnetization of the Mn ions is calculated using mean-field theory[25], and the z component of the average Mn spin, $< S_z >$ is determined by solving

$$< S_z >= SB_s\{\frac{gS}{kT}[\mu_B B - \frac{3kT_c < S_z >}{gS(S+1)}]\} \qquad (1)$$

where g is the free electron g-factor, B_s is the Brillouin function, S = 5/2 is the spin of the magnetic Mn ion and T_c = 330 K is the Curie temperature. Figure 7 shows the calculated band structure for $\mathrm{In}_{0.96}\mathrm{Mn}_{0.04}\mathrm{As}$ at 290 K for $T_c = 300$ K. We see that the ferromagnetic order of the Mn ions causes spin splitting of the bands. The red arrows in Fig. 7, show the optical transitions that are possible for an 800 *nm* pump pulse. We see that transitions are possible from the heavy-hole, light-hole and spin-orbit split valence bands. Furthermore, the transitions from the heavy and light hole create photoexcited electrons in the conduction band that are above the energy threshhold for scattering into the satellite L valleys. These electrons rapidly scatter into the satellite valleys (which have a large effective mass and hence a greater density of states) and take a long time to return to the Γ valley and then relax to the bottom of the Γ valley, similar to the 620 *nm* photoexcitation in GaAs.[26–28]

5. CONTRIBUTIONS TO THE DIFFERENTIAL TRANSMISSION SPECTRA.

The time resolved differential transmission (DT) measures *changes* to the absorption of the probe pulse that result from the pump pulse. For thin samples, $\Delta T/T \approx -\Delta\alpha\, L$ where L is the thickness of the sample and $\Delta\alpha$ is the change in the absorption coefficient. While a detailed understanding of the absorption changes requires using the semiconductor Bloch equations,[29] one can gain insight into what types of processes influence the DT signal by looking at a simplified, approximate expression for the absorption coefficient:

$$\alpha(\omega,t)=\frac{1}{\omega}\int d\omega'\int dt'\,N(\omega',t-t')\sum_{\text{transitions}}\int dk\,\underbrace{|H_k|^2}_{\substack{\text{optical}\\ \text{matrix}\\ \text{element}}}$$

$$\times\delta(\underbrace{\varepsilon_c(k)-\varepsilon_v(k)}_{\substack{\text{electron and hole}\\ \text{energies}}}-\omega')[1-\underbrace{f_c^e(k,t')-f_v^h(k,t')}_{\substack{\text{electron and hole}\\ \text{distribution functions}}}]. \tag{2}$$

Here, $\alpha(\omega,t)$ is the absorption of the probe pulse centered at frequency ω as a function of delay time t with respect to the pump pulse, $N(\omega',t)$ is the transient photon energy density of the probe pulse, $H_{kk'}$ is the optical matrix element between conduction and valence band states, and $f_c^e(k,t')$, $f_v^h(k,t')$ are the electron and hole distribution functions in the conduction and valence bands respectively.

There are four main contributions to the differential transmission signal $-\Delta T/T_0 = (T_0 - T)/T_0$[30]. These can be understood by looking at changes in the absorption coefficent of the probe, eq. 2 above, and seeing what changes as a result of the pump pulse. The four main contributions are: 1)**Phase-Space Filling**: This comes from the probe pulse creating additional electrons and holes that block the absorption of additional carriers from the probe pulse by the *Pauli exclusion principal.* One can not create an additional electron-hole pair with the probe pulse if the pump pulse has already created one since the Pauli principle excludes two electrons from being in the same state. As the photoexcited carriers relax, the absorption of the probe pulse increases with time. Phase space filling gives a negative contribution to $-\Delta T/T_0$ (provided there is no carrier inversion before the pump pulse). 2) **Band Gap Renormalization**: This results from the pump pulse photoexciting electron-hole pairs, which through the many-body interactions, cause the electron and hole energies (in the delta function in eq. 2) to change. This causes the band gap to shrink. Band gap renormalization gives a positive contribution for probe laser energies *below* the pump-induced photoexcited carriers and a negative contribution at energies *above* the pump-induced photoexcited carriers. This affect tends to be strong just below the band edge. With no pump-pulse, probing below the band edge will not lead to absorption of the probe pulse. However, with a pump-pulse, the band-gap narrows and the probe pulse will now be absorbed. 3) **Local Field Effects**: Photoexcited electon-hole pairs interact through the Coulomb interaction. This leads to the formation of excitons and changes to the electron and hole wavefunctions. (Even states excited above the band gap are *unbound excitons*). These changes to the wavefunctions will change the op-

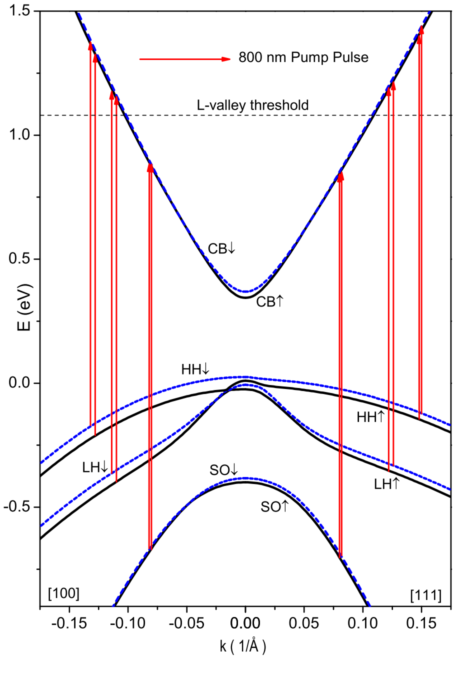

FIG. 7: Electronic structure of $In_{0.96}Mn_{0.04}As$ at T= 290 K for B =0. The energy bands are spin-split due to the ferromagnetism. The allowed optical ransitions for a pump wavelength of 800 nm (1.55 eV) are shown by the (red) arrows. The dotted line at 1.08 eV shows the threshold for Γ valley electrons to scatter to the satellite L valley.

tical matrix elements in eq. 2 and lead to a *Coulomb Enhancement* of the absorption of the probe pulse. Now with a pump-pulse on, additional electron-hole pairs are created which screen the Coulomb interaction and change the optical matrix elements. This gives a negative contribution at energies below the photoexcited carriers and a positive contribution at energies above the photoexcited carries. 4) **Free Carrier Absorption**: This is due to the *intraband* absorption of the photoexcited carriers (which must be assisted by phonons or impurities). This will give a positive contribution to $-\Delta T/T_0$ due to the photoinduced absorption.

Figure 8 shows the calculated bands of In ${}_{0.96}$Mn$_{0.04}$As at 290 K for $T_c = 300$ K. This time we show the transitions from the probe pulse. This allows us to see which regions are being monitored by the probe pulse. Transitions are shown for probe wavelengths of 3.5 μm (black arrows) and 2 μm (red arrows). We see that the 3.5 μm probe primarily probes the states at or near the band edge while the 2.0 μm probe is deep into the bands. This can explain the sign change in the differential transmission signal shown in Fig. 5.

¿From Fig. 8, we see the reason for the change of the sign between 3.5 μm and 2 μm. The 2 μm probes deep into the bands were the phase space filling contribution to $-\Delta T/T_0$ is dominant. However, the 3.5 μm transitions probe close to and slightly below the band edge. In this case, the band gap renormalization term will dominate and give a positive signal to $-\Delta T/T_0$. In addition, free carrier absorption can also contribute to the observed positive signal at 3.5 μm.

In summary, we probed and tuned the carrier dynamics in the MOVPE grown InMnAs. In contrary to the reported studies in the MBE grown InMnAs, focused on narrower pump/probe schemes[12], the TRDT measurements in this work demonstrated that the carrier relaxation time can be tuned and last longer than a few ps, when the excited carrier are close or above the L-valley threshold. In addition, we observed the change in the nature of the dynamical processes, switched between the photoinduced absorption and bleaching in a ferromagnetic semiconductor. We have calculated the electronic structure for InMnAs using an 8 band **k**·**p** model which includes the nonparabolicity and coupling of the electrons and holes to the Mn impurities, to model the observed dynamics. The calculated band structure with the bands splitting due to the Mn impurities shows that: 1) The 800 *nm* pump pulse creates photoexcited carriers from all the hole bands and some of the photoexcited electrons can scatter to the satellite L valleys which slows down the relaxation of the electrons. 2) The sign change between probing with 3.5 μm and 2.0 μm can be explained by what regions of the bands are sampled by the probe pulses. At 2.0 μm the probe is deep into the bands where the *phase space filling* term dominates. At 3.5 μm, the probe is right at and slightly below the band-edge where band-gap renormalization dominates.

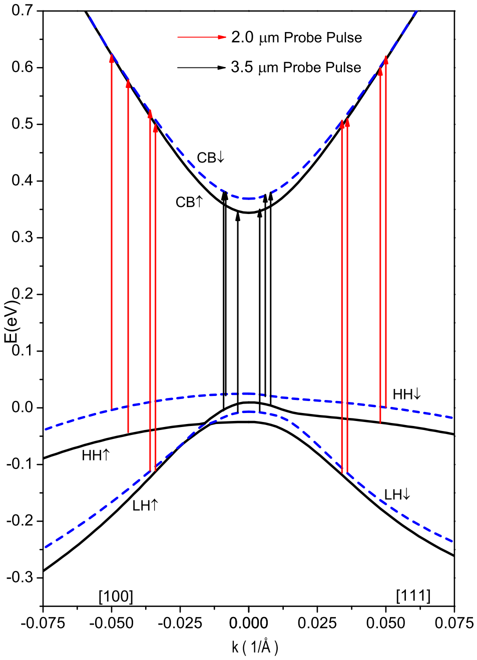

FIG. 8: Electronic structure of $In_{0.96}Mn_{0.04}As$ at T= 290 K for B =0. The energy bands are spin-split due to the ferromagnetism. The allower optical transitions are shown for a *probe* wavelength of 3.5 μm (black arrows) and 2.0 μm (red arrows).

Acknowledgment: This work has been supported by the National Science Foundation through grants Career Award DMR-0846834, DMR-0800479, DMR-0706313, DMR-1105437, and by the National High Magnetic Field Laboratory through a UCGP.

---

[1] T. Schallenberg and H. Munekata, H., Appl. Phys. Lett. **89**, 042507 (2006).

[2] A. J. Blattner, and B. W. Wessels, Appl. Surf. Science, **221**,155 (2004).

[3] A. J. Blattner, P. L. Prabhumirashi, V. P. Dravid, and B. W. Wessels Journal of Crystal Growth **259**, 8 (2003).

[4] N. Rangaraju, Li Pengcheng, and B. W. Wessels, Phys. Rev. B **79**, 205209(2009).

[5] N. D. Parashar, N. Rangaraju, V. K. Lazarov, S. Xie, and B. W. Wessels Phys. Rev. B **81**, 115321 (2010).

[6] P. T. Chiu, S. J. May, and B. W. Wessels, Appl. Phys. Lett., **85**, 780 (2004).

[7] G. A. Khodaparast, M. Frazier, R. N. Kini, K. Nontapot, T. D. Mishima, M. B. Santos, B. W. Wessels, Proc. of SPIE, Vol. 7608, 76080O-1 (2010).

[8] G. A. Khodaparast, M. Bhowmick, T. D. Mishima, M. B. Santos, C. Feaser, B. W. Wessels Spintronics III, Proc. of SPIE, Vol 7760, 77600X-1 (2010).

[9] M. Bhowmick, T. R. Merritt, K. Nontapot, B. W. Wessels, O. Drachenko, G. A. Khodaparast, Physics Procedia **3**, 1167 (2010).

[10] M. Frazier, K. Nontapot, R. N. Kini, G. A. Khodaparast, T. Wojtowicz, X. Liu, J. K. Furdyna, Appl. Phys. Lett. **92**, 06191(2008).

[11] K. Nontapot, R. N. Kini, A. Gifford, T. R. Merritt, G. A. Khodaparast, T. Wojtowicz, X. Liu, J. K. Furdyna, Appl. Phys. Lett. **90**, 143109 (2007).

[12] J. Wang, C. Sun, Y. Hashimoto, Y., Kono, J. , Khodaparast, G. A., Cywinski, L., Sham, L. J., Sanders, G. D. , Stanton, C. J., and Munekata, H., "Ultrafast magneto-optics in ferromagnetic III-V semiconductors," Journal of Physics: Condens. Matter, **18**, R501 (2006).

[13] J. Wang, G. A. Khodaparast, J. Kono, A. Oiwa, and H. Munekata, Journal of Modern Optics **51**, 2771 (2004).

[14] R. N. Kini,K. Nontapot, G. A. Khodaparast, R. E. Welser, and L. J. Guido, Journal of Applied Physics **103**, 064318 (2008)

[15] P.P. Paskov and L.I. Pavlov, Appl. Phys. B **54**, 113(1992).

[16] Semicond. Sci. Technol. **7**, 124 (1992).

[17] T. Tsai, c. Chang, S. Gwo, Appl. Phys. Lett. **90**, 252111 (2007).

[18] M. Ulman, D. W. Bailey, L. H. Acioli, F. G. Vallee, , Stanton, C. J., Ippen, E. P., and Fujimoto, J. G., Phys. Rev. B 47, 10267-10278 (1993).

[19] Kuznetsov, A. V., Kim, Chang Sub, Stanton, C. J., J. Appl. Phys. 80, 5899-5908 (1996).

[20] U. Siegner, R. Fluck, G. Zhang, and U. Keller, Appl. Phys. Lett **69**, 2566 (1996).

[21] S. Kim, E. Oh, J. U. Lee, D. S. Kim, S. Lee, J. K. Furdyna ,Appl. Phys. Lett **88**, 262101 (2006).

[22] G. A. Khodaparast, J. Kono, Y. H. Matsuda, S. Ikeda, N. Miura, Y. J.Wang, T. Slupinski, A. Oiwa, H. Munekata, Y. Sun, F. V. Kyrychenko, G. D. Sanders, and C. J. Stanton, Physica E **21**, 978 (2004).

[23] G. D. Sanders, F. V. Kyrychenko, Y.Sun, C. J. Stanton, G. A. Khodoparast, J. Kono, Y. H. Matsuda, N. Miura, T. Slupinski, A. Oiwa, and H. Munekata, Phys. Rev. B. **68**, 165205 (2003).

[24] M. Zudov,J. Kono, Y. H. Matsuda, T. Ikaida, N. Miura, H. Munekata, G. D. Sanders, Y. Sun, and C. J. Stanton , Phys. Rev. B **66**, 161307(R)(2002).

[25] N. W. Ashcroft and N. D. Mermin, Solid State Physics (Saunders College, Philadelphia, 1976), pp. 715-718.

[26] C. J. Stanton, D.W. Bailey and K. Hess, Phys. Rev. Lett. **65** 231 (1990).

[27] D. W. Bailey, C. J. Stanton and K. Hess, Phys. Rev. B **42** 3423 (1990).

[28] C. J. Stanton and D. W. Bailey, Phys. Rev. B **45** 8369 (1992).

[29] H. Haug and S. Koch, Quantum theory of the optical and electronic properties of semiconductors, 1990, World Scientific, Singapore

[30] K. El Sayed, and C. J. Stanton, Phys. Rev. B **55** 9671 (1997).